J. Fluid Mech. (1998), *vol.* 372, *pp.* 93–118. Printed in the United Kingdom

The influence of rotational and vibrational energy relaxation on boundary-layer stability

By FABIO P. BERTOLOTTI

DLR Institut für Strömungsmechanik, Göttingen, Germany

(Received 2 March 1998 and in revised form 18 May 1998)

We investigate the influence of rotational and vibrational energy relaxation on the stability of laminar boundary layers in supersonic flows by numerically solving the linearized equations of motion for a flow in thermal non-equilibrium. We model air as a mixture of nitrogen, oxygen and carbon dioxide, and derive accurate models for the relaxation rates from published experimental data in the field of physical chemistry. The influence of rotational relaxation is to dampen high-frequency instabilities, consistent with the well known damping effect of rotational relaxation on acoustical waves. The influence of rotational relaxation can be modelled with acceptable accuracy through the use of the bulk-viscosity approximation when the bulk viscosity is computed with a formula described herein. Vibrational relaxation affects the growth of disturbances by changing the characteristics of the laminar mean flow. The influence is strongest when the flow field contains a region at, or near, stagnation conditions, followed by a rapid expansion, such as inside wind tunnels and around bodies with a blunt leading edge, whereby the rapid expansion causes the internal energy to freeze in a distribution out of equilibrium. For flows at Mach 4.5 and stagnation temperature of 1000 K, the total amplification exhibited by boundary-layer disturbances over a sharp flat plate in wind-tunnel flows can reach a value that is fifty times as high as the value computed under the assumption of thermal equilibrium. The difference in amplification can be twice as high in the case of a blunt flat plate at atmospheric flight conditions.

1. Introduction

The present investigation looks at the influence of molecular rotational and vibrational energy non-equilibrium (i.e. thermal relaxation processes) on the instability of boundary layers in supersonic flows. The motivation for this work comes from two sources. First, within the field of acoustics (e.g. Thompson 1988; Bauer 1965; Bass *et al.* 1984) one can experimentally measure the increase in the damping rate of high-frequency acoustical waves in polyatomic gases compared to that in monoatomic gases, even at room temperature and pressure. The increase in damping rate is due to a phase lag of the rotational and vibrational energy with respect to the translational energy. Since in supersonic boundary layers the instabilities can reach frequencies into the megaHertz range, it is natural to question if relaxation processes can affect their growth. Secondly, at supersonic flow velocities the vibrational energy is essentially frozen in the free stream and in equilibrium with translational energy at the wall, leading to a boundary layer with characteristics different from those computed with the assumption of thermal equilibrium. Thus, it is also natural to question if vibrational relaxation processes influence the growth of boundary-layer instabilities.

In a recent and carefully conducted experiment, Nerushev & Novopashin (1997) have measured the influence of acoustical-wave attenuation on the location of laminar–turbulent transition in pipe flow. Measurements were made of the friction factor in a pipe carrying a flow of either nitrogen or carbon monoxide. These two gases were chosen because they have nearly identical thermodynamic and transport properties, leading the authors to attribute the difference in acoustical-wave attenuation to a difference in the rotational relaxation time in the two gases.† The authors claim that the transition Reynolds number in nitrogen is about 10% lower than that in carbon monoxide, although the data are a bit noisy. This result suggests that rotational relaxation influences the growth of flow instabilities, even at room temperature and pressure.

The influence of chemical, rather than thermal, non-equilibrium on boundary-layer stability has been addressed in some recent studies (cf. Stuckert 1991; Stuckert & Reed 1994; Chang, Vinh & Malik 1997; Hudson, Chokani & Candler 1997). These numerical studies show that chemical non-equilibrium stabilizes the flow, in agreement with the experimental measurements of Germain & Hornung (1997) made over a slender sharp cone in hypersonic flow. Of most relevance is the study of Hudson *et al*., which avoids the assumption of thermal equilibrium and includes the effect of vibrational energy relaxation. The study shows that vibrational relaxation has a slight stabilizing influence on second-mode instability waves in a boundary layer created by a free-stream flow at Mach 10 and in thermal equilibrium.

All the above results suggest that relaxation processes have a general stabilizing influence on boundary-layer stability. Our work shows that such a conclusion may be correct with regard to rotational energy relaxation, but it is false for vibrational energy relaxation. The basic reason for this difference stems from the widely different relaxation rates of these two processes. The rotational energy of nitrogen and oxygen relaxes to equilibrium within five to ten molecular collisions, cf. Gaydon & Hurle (1963), and the associated rotational relaxation time is much shorter than the characteristic time taken by a particle to travel a distance of the order of the thickness of a boundary layer. Hence, rotational relaxation affects the oscillatory motion of high-frequency instabilities, but not the steady laminar mean flow.

In contrast, the vibrational energy needs three to five orders of magnitude, cf. Parker (1959), more collisions to relax to equilibrium than rotational energy, and the associated Damköhler number $U\tau/L$, based on free-stream velocity U, body dimensions L and relaxation time τ, is much greater than one for bodies in atmospheric flight or in wind-tunnel flows. (The Damköhler number is essentially a Knudsen number in which the time between collisions is replaced by the relaxation time.) At first sight, then, it may seem appropriate to consider the vibrational energy as frozen, and to hold its value constant over the entire flow field. However, such an approximation is incorrect because the efficient energy exchange between the vibrational modes of the gas molecules and the vibrational modes of the atomic lattice of the wall material tends to rapidly bring the flow in the near wall region into thermal equilibrium. The vibrational energy develops a boundary layer of its own, which affects the overall characteristics of the laminar boundary layer, including its stability. Furthermore, the free-stream value to which the vibrational temperature

† The authors quote $Z^{\mathrm{rot}} = 2.3$ for CO and $Z^{\mathrm{rot}} = 6.0$ for N_2, which implies a lower bulk viscosity value for CO in comparison to N_2. However, the authors also quote a higher sound-damping coefficient for CO and attribute the higher value to a correspondingly higher value of the bulk viscosity of CO with respect to N_2. This inconsistency is not clarified in their paper.

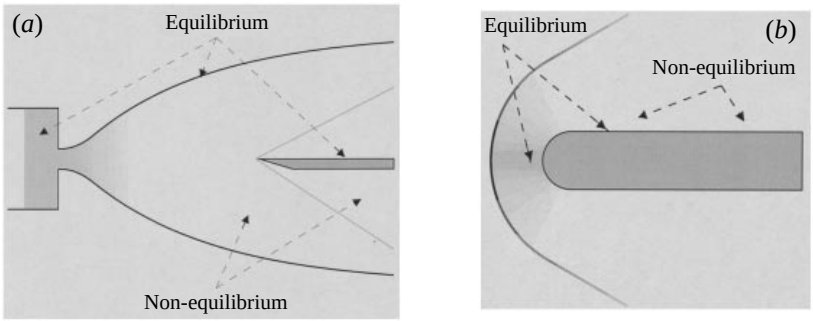

FIGURE 1. Regions of equilibrium and non-equilibrium vibrational energies (*a*) in a wind tunnel and (*b*) over a blunt body in free flight. Equilibrium regions are characterized by low flow velocities and high temperatures, and include the supply chamber, the stagnation region, and the immediate neighbourhood of a solid wall. Non-equilibrium flow is generated in regions having a rapid flow expansion, such as the rapid expansion in the nozzle and around the blunt leading edge. The rapid expansion freezes the vibrational energy at a level close to the stagnation temperature, leading to non-equilibrium flow downstream.

asymptotes outside the boundary layer strongly depends on the upstream history of the flow (see figure 1). In particular, the free-stream value depends on whether the fluid particles come from a high-temperature region, such as the supply chamber in supersonic wind tunnels and the stagnation region of blunt bodies, or from a low-temperature region such as the free stream in flight conditions when only weak oblique shocks are present. Herein, we show that in a flow at Mach 4.5 and stagnation temperature of 1000 K, the total amplification exhibited by boundary-layer disturbances over a sharp flat plate in wind-tunnel flows can reach a value that is fifty times as high as the value computed under the assumption of thermal equilibrium, while the difference in amplification can be twice as high in the case of a blunt flat plate at atmospheric flight conditions.

The influence of thermal relaxation processes on flow stability also depends on the degree to which the rotational and vibrational energies are excited. Rotational energy is fully excited above 50 K, hence it is always activated in flows around vehicles in atmospheric flight. In contrast, the characteristic vibrational temperatures of nitrogen and oxygen are above 2000 K, and the contribution of the vibrational energy mode to the total internal energy exceeds 10% in oxygen, air, and nitrogen at temperatures above 500, 700 and 800 K, respectively. Below these temperatures, the state of the vibrational energy, whether in equilibrium or relaxing, has little influence on stability. Consequently, the vibrational energy relaxation process becomes important when the stagnation temperature in the flow surpasses about 800 K.

The first part of this paper deals with the physical modelling of rotational and vibrational relaxation. We derive models for the relaxation rates from published experimental data in the field of physical chemistry. The models are valid in the temperature range of 220 to 1400 K, and the model for rotational relaxation gives rise to a bulk-viscosity coefficient with a temperature dependence that differs from that used in previous stability analyses.

In the second part of this paper, which presents the influence of rotational relaxation on the amplification of second-mode instabilities, and the third part, which presents the influence of vibrational relaxation of both first-mode and second-mode instabilities, we focus mainly on a flow at Mach number of 4.5 and at the atmospheric conditions existing at 12 000 m altitude. This flow is chosen because its stagnation temperature

of 1041 K is high enough to significantly excite the vibrational energy of nitrogen and oxygen, but is too low to cause any appreciable dissociation.

In order to limit the length of this manuscript, details that are not central to the disclosure of the main results are omitted, including equations that can be derived using known and documented steps. For a more lengthy and complete presentation the reader is referred to Bertolotti (1997).

2. Physical modelling

We use the equation of Landau & Teller (1936) to model the relaxation process of both rotational and vibrational energy,

$$\frac{\mathrm{d}\, e^*}{\mathrm{d}\, t} = \frac{1}{\tau}\left(\bar{e} - e^*\right), \tag{2.1}$$

where e^* denotes the actual internal energy contained in the excited state and $\bar{e}$ denotes the energy that would be contained in the excited state if the gas were in equilibrium. The relaxation time τ controls the rate at which the energy departure from equilibrium relaxes to its initial value.

Although the Landau–Teller equation is considered an accurate model for relaxation processes when only the first few quantum states are significantly populated (for example, when the harmonic oscillator model for vibrational motion is valid), we can only assume that this equation is an accurate model for rotational relaxation since many rotational quantum states are populated at room temperature. Furthermore, the description of the excited energy state by a single scalar, as appears in (2.1), implies the existence of a Boltzmann distribution in energy. Studies (Raff & Winter 1968) employing the master equation to model energy transitions between individual rotational quantum levels show that the use of a single rotational relaxation time is a gross oversimplification in the case of hydrogen. Hydrogen is, of course, an exceptional gas, whose small molecular moment of inertia produces relaxation times two orders of magnitude higher than those of nitrogen and oxygen. For nitrogen and oxygen, experiments on rotational relaxation in a shock wave at Mach 7.0 (Robben & Talbot 1966) and in a jet of pure nitrogen gas (Yamazaki, Masahiro & Yoshiyasu 1981) and of a helium and nitrogen mixture (Belikov & Sharafutdinov 1995) expanding into quasi-vacuum have also measured a rotational energy distribution that is non-Boltzmann. However, these experiments also show that the energy distribution can be closely approximated by *two* Boltzmann distributions, one for the lower (e.g. 50) rotational quantum states and one for the higher ones, each distribution being characterized by a different temperature. At the translational temperatures below 1400 K that are of interest here, practically all of the rotational energy is contained in the lower quantum states, and, thus, the use of a single rotational temperature and the Landau–Teller equation for rotational relaxation is adequate for our purposes.

2.1. *The rotational relaxation rates*

The rotational relaxation time τ^{rot} can be expressed as the product of the mean time between molecular collisions C and the number of molecular collisions Z^{rot} needed for relaxation,

$$\tau^{\mathrm{rot}} = C\, Z^{\mathrm{rot}}. \tag{2.2}$$

Estimates of Z^{rot} inferred from laboratory measurements are sufficiently consistent to extract an average, representative value. For nitrogen, absorption measurements

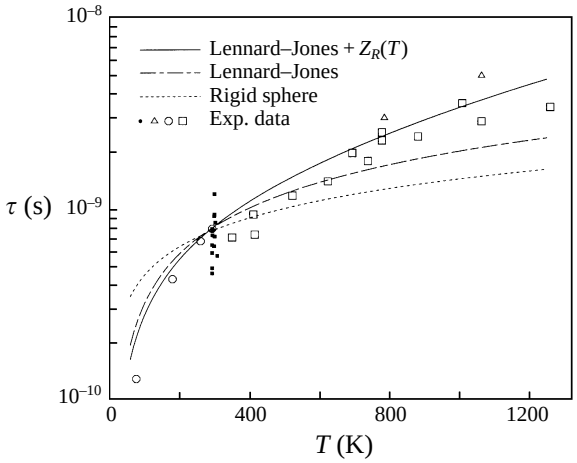

FIGURE 2. Comparison of the relaxation time τ given by theory and experiment for pure nitrogen at one atmosphere.

of ultrasonic sound have yielded values of 5.26 collisions (Greenspan 1959) and 5.5 collisions (Andersen & Horning 1959), while shock-wave measurements using the electron-beam fluorescence technique (Robben & Talbot 1966) have yielded $Z^{\text{rot}} = 5$, and recovery-factor measurements (O'Neal & Brokaw 1963) have yielded $Z^{\text{rot}} = 7.3$. For oxygen, ultrasonic measurements have yielded 13 collisions (Connor 1958) and 4.09 collisions (Greenspan 1959), while the recovery factor measurements have yielded 12 collisions (O'Neal & Brokaw 1963) In our work we use $Z^{\text{rot}} = 5.5$ for nitrogen in a nitrogen bath, and $Z^{\text{rot}} = 10$ for oxygen in an oxygen bath at a translational temperature of 300 K.

Theoretical models based on quantum theory (Brout 1954), on classical kinetic theory (Parker 1959), and numerical solutions to the master equation (Raff & Winter 1969) predict an increase of the rotational collision number Z^{rot} with temperature. Because these *ab initio* quantum-mechanical calculations are approximate in nature, and because the scope of the present work is focused on macro-mechanical gas behaviour, we use herein the following empirical dependence for $Z^{\text{rot}}(T)$, which we construct from a fit of the available experimental data:

$$Z^{\text{rot}}(T) = Z_0^{\text{rot}} \exp\left[\frac{T - 293.3}{20\,\epsilon/k}\right], \tag{2.3}$$

where T is the translational temperature, Z_0^{rot} is the collision number measured at room temperature, and ϵ/k is the ratio of the Lennard–Jones potential-well depth to Boltzmann constant. The relaxation time computed using (2.3) and using C computed with the Lennard–Jones potential is compared with experimental data in figure 2. Also shown in this figure are the results obtained with the Lennard–Jones or a rigid sphere model together with the constant value of $Z^{\text{rot}} = Z_0^{\text{rot}}$.

From (2.3) we can obtain an expression for the bulk viscosity μ_{v} using the known relationship between μ_{v} and τ (e.g. Clarke & McChesney 1964; Pierce 1981; Vincenti & Kruger 1965). The bulk viscosity is not a physical property of a gas, but rather, an approximation designed to simulate the effect of thermal relaxation when the governing equations are cast in terms of a single temperature. The bulk viscosity also approximates the effect of long-range intermolecular forces in high density gases and in fluids, but this aspect is not relevant here. The approximation is based on the

assumption that the time scale of the macroscopic gas motion (i.e. the flow velocity) is significantly longer than the relaxation time of the molecular internal degree of freedom.

The first investigator to have included the bulk viscosity in the boundary-layer stability equations seems to have been Mack (1965). Mack chose a constant value of $\mu_v/\mu = 0.8$, which is higher than the 0.6 reported for air at room temperature (e.g. Thompson 1988). This difference in value may indicate that Mack chose to model air at a higher temperature, as we show below. Subsequent investigators have either used Mack's value or have invoked Stokes hypothesis, setting the value to zero. Our expression for the bulk viscosity is accurate over a temperature range from 200 to 1400 K, and offers an alternative choice.

Below 1400 K the vibrational energy relaxation is much slower than that of the rotational energy, so the rotational energy contribution to the bulk viscosity is dominant and the vibrational energy contribution is herein neglected. Noting that the factor ϵ/k in (2.3) is about 97 K for air, 92 K for nitrogen and 113 K for oxygen, we can simply set this factor equal to the constant 97 K. This leads to the following expression for the bulk viscosity, valid for air, nitrogen and oxygen:

$$\frac{\mu_v(T)}{\mu(T)} = \left(\frac{\mu_v}{\mu}\right)_{T=293.3\text{K}} \exp\left[\frac{T-293.3}{1940}\right], \tag{2.4}$$

where T is in Kelvin. This expression yields a ratio $\mu_v/\mu = 0.8$ at 1000 K, which agrees with Mack's value. More generally, the expression yields a ratio μ_v/μ that varies from 0.57 to 1 within the temperature range of 200 to 1200 K.

2.2. *The vibrational relaxation rates*

The vibrational relaxation time for pure nitrogen and pure oxygen at standard pressure and temperature is about 1 s and 0.1 s, respectively. Carbon dioxide, on the other hand, has vibrational relaxation times in the order of 10^{-5} s at the same conditions. Furthermore, the characteristic vibrational temperature of nitrogen, $T^{\text{vib}}_{N_2} = 3354$ K, and of the asymmetric stretching mode of carbon dioxide, $T^{\text{vib}}_{CO_2} = 3380$ K, have almost the same value. These two facts combine to produce a strong sensitivity of the vibrational relaxation time of nitrogen to the presence of small concentrations of carbon dioxide. The reason behind this catalytic effect lies in a resonant vibrational energy exchange (V-V transfer) that occurs with much higher probability at each molecular collision than a vibrational-translational energy (V-T) transfer: the nitrogen exchanges vibrational energy with carbon dioxide at almost every collision, and the carbon dioxide then relaxes with a (V-T) exchange at its normal fast rate.

In Bertolotti (1997) a model is derived for the relaxation rates of nitrogen and oxygen in the presence of carbon dioxide and water vapour by considering 17 reactions involving the first vibrational state of nitrogen and oxygen and the symmetric stretch, asymmetric stretch and bending modes of carbon dioxide and water vapour, plus the rotational energy of water vapour. The relaxation problem is governed by a coupled system of first-order differential equations, as described by Herzfeld & Litovitz (1959). The relaxation rates appear as the eigenvalues of the system. For a generic mixture, the eigenvalues cannot be associated with the relaxation rates of any one particular component alone (Shuler 1959); however, due to the short relaxation times of carbon dioxide and water vapour in comparison to those of nitrogen and oxygen, the relaxation process proceeds on two widely different time scales, one governing the relaxation of CO_2 and H_2O in which N_2 and O_2 play a minor role, the other governing the relaxation of N_2 and O_2 in which carbon dioxide and water vapour play the role

Reaction			C_1 (s atm)$^{-1}$	C_2 (K$^{1/3}$)	References For C_1	References For C_2
$N_2^* + N_2$	$(k_{010} \rightleftharpoons k_{001})$	$N_2 + N_2$	1	−140	EBS	GH
$N_2^* + O_2$	$(k_{020} \rightleftharpoons k_{002})$	$N_2 + O_2$	1	−140	EBS	B97
$N_2^* + CO_2$	$(k_{030} \rightleftharpoons k_{003})$	$N_2 + CO_2$	1	−140	EBS	B97
$N_2^* + CO_2$	$(k_{060} \rightleftharpoons k_{006})$	$N_2 + CO_2^*$ $(v3)$	1.4×10^7	+30	Pack	Pack
$O_2^* + N_2$	$(k_{110} \rightleftharpoons k_{101})$	$O_2 + N_2$	40	−105	EBS	B97
$O_2^* + O_2$	$(k_{120} \rightleftharpoons k_{102})$	$O_2 + O_2$	63	−105	Monk	VK
$O_2^* + CO_2$	$(k_{130} \rightleftharpoons k_{103})$	$O_2 + CO_2^*$ $(v2)$	3.0×10^5	−67	EBS	B97
$CO_2^*(v3) + N_2$	$(k_{310} \rightleftharpoons k_{301})$	$CO_2^*(v2) + N_2$	7.0×10^4	−60	EBS	B97
$CO_2^*(v3) + O_2$	$(k_{320} \rightleftharpoons k_{302})$	$CO_2^*(v2) + O_2^*$	7.5×10^4	−60	EBS	RG
$CO_2^*(v3) + CO_2$	$(k_{330} \rightleftharpoons k_{303})$	$CO_2^*(v2) + CO_2$	1.5×10^5	+5	EBS	B97

TABLE 1. Reaction-rate constants for various energy exchanges. The stars indicate a molecule with the first vibrational state excited. The author names or initials in the References columns are: EBS, Evans, Bass & Sutherland (1971); Pack (1980); Monk (1969); GH, Gaydon & Hurle (1963); B97, Bertolotti (1997); VK, Vincenti & Kruger (1965); RG, Rosser & Gerry (1969).

of a catalyst. Consequently, two eigenvalues can be associated with the relaxation of nitrogen and oxygen in our particular gas mixture. These eigenvalues, plus the associated eigenvectors, lead to the following relaxation equations for nitrogen and oxygen:

$$\frac{1}{\tau_{N_2}} = k_{010}Z + k_{020}Y + +(k_{030} + k_{060})X - k_{006}Z x_{10}, \tag{2.5a}$$

$$\frac{1}{\tau_{O_2}} = k_{110}Z + k_{120}Y + (k_{130} + k_{302})X - k_{320}Y x_{20}, \tag{2.5b}$$

where

$$\begin{aligned} a &= (k_{220} + k_{005})Z + (k_{210} + k_{105})Y + k_{304}\xi X, \\ d &= (k_{310} + k_{006})Z + k_{320}Y + k_{330}X, \\ f &= k_{060}X, \quad h = k_{302}\xi X, \\ x_{10} &= (af)/(ad), \quad x_{20} = (ah)/(ad), \end{aligned}$$

and where Z, Y, X are the molar concentrations of nitrogen, oxygen, and carbon dioxide at the ground state, and the corresponding lower case letters are the concentrations in the vibrationally excited state. The reaction rate constants k are discussed below. The variable $\xi = 2\exp[-960/T]$ is the percentage of CO_2 atoms with the doubly-degenerate bending mode excited, and arises from the assumption that this mode is in equilibrium (Henderson *et al.* 1968). We have omitted the terms due to water vapour since the trace amount of water vapour at the selected flow conditions under consideration here is negligible. The reaction rate constants k have a temperature dependency of the form (e.g. Herzfeld & Litovitz 1959; Vincenti & Kruger 1965; Anderson 1989)

$$k = C_1 \exp\left[C_2\left(T^{-1/3} - 300^{-1/3}\right)\right], \tag{2.6}$$

where T is the translational temperature in Kelvin. The values of the coefficients C_1 and C_2 for each reaction are shown in table 1.

The values of C_1 were either taken directly from, or computed from the experimental

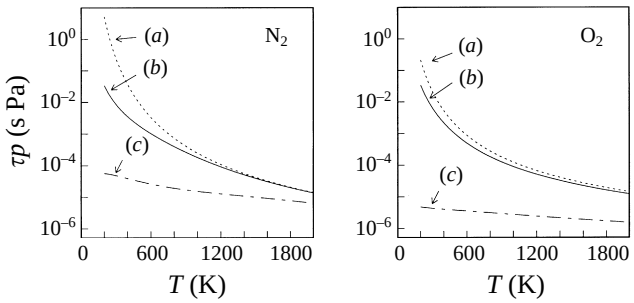

FIGURE 3. Product of vibrational relaxation time τ and pressure p for nitrogen and oxygen as function of temperature: (*a*) air model composed of 0.77783 N_2 and 0.22217 O_2 mole fractions (*b*) air model including 0.0003 mole fraction of CO_2, (*c*) air model including 1% mass fractions of CO_2 and H_2O.

data given within the references listed in the table. Because many of the experimental measurements were conducted at room temperature, the value of the constant C_2 for some of the reactions listed above was, unfortunately, not available within the survey of publications done by the author. To obtain an estimate of the value of C_2 for V-T reactions involving at least one bi-atomic molecule and not involving water vapour, we use the linear dependence of C_2 on the energy $\Delta\epsilon$ exchanged in the reaction. This linear dependence is predicted by the model of Herzfeld & Litovitz (1959) based on the theory of Landau & Teller (1936). The values of C_2 in table 1 associated with the reference B97 have been obtained with this linear relation. The relaxation time τ_{N_2} computed with the reaction rates of table 1 are in good agreement with the experimental data of Henderson *et al.* (1968) for a set of mixtures with different concentrations of nitrogen, carbon dioxide and water vapour at a temperature of 450 K.

We model dry air as a composition of 0.7776 (mole fraction) nitrogen, 0.2221 oxygen, and 0.0003 carbon dioxide. The concentration of carbon dioxide agrees with current atmospheric levels. In figure 3 we show the relaxation times computed by our model for the temperature range of 200 to 1900 K. The strong effect of small quantities of carbon dioxide on the relaxation of nitrogen can be seen by comparing lines (*a*) and (*b*), whose corresponding gas mixtures differ from each other by only 300 parts per million of carbon dioxide. In addition, line (*c*) shows the results for a 'wet' mixture having a high concentration of carbon dioxide and water vapour. The strong sensitivity of τ_{O_2} to water vapour comes from a second resonant energy exchange involving the bending mode of H_2O (2295 K) and the vibrational mode of oxygen (2273 K). We have included this particular wet gas mixture in the figure to highlight the synergistic influence of CO_2 and H_2O on the relaxation rates of nitrogen and oxygen, although this particular mixture is more representative of the flow conditions around a turbine blade within a jet engine than those around a wing in atmospheric flight.

3. The governing equations

The vibrational energy of carbon dioxide is assumed to be in equilibrium, in view of the rapid relaxation rates shown in table 1. The rotational energy is also assumed to be in equilibrium since the concentration of this species is small. This leaves the density ρ, velocity $\boldsymbol{v}$, pressure p, translational temperature T, and the rotational and

vibrational temperatures of nitrogen and oxygen, $T_{N_2}^{\mathrm{rot}}$ $T_{O_2}^{\mathrm{rot}}$ $T_{N_2}^{\mathrm{vib}}$ $T_{O_2}^{\mathrm{vib}}$, as independent variables.

The Navier–Stokes equations are changed in essentially two ways to incorporate thermal non-equilibrium. First, the relaxation equations for the vibrational and for the rotational temperatures of nitrogen and oxygen are introduced. Secondly, the heat-flux vector is extended to include the diffusion of vibrational and rotational energies that takes place in the presence of the corresponding temperature gradients.

The Eulerian form of the relaxation equation (2.1), for either rotational or vibrational energy, takes the form

$$\rho \frac{\mathrm{D}e_i^*}{\mathrm{D}t} + \frac{\rho}{\tau}(e_i^* - \bar{e}_i) = -\mathrm{div}[\boldsymbol{q}_i^*], \tag{3.1}$$

where $e_i^*, \bar{e}_i$ and τ have the same meaning as in (2.1), and $\boldsymbol{q}_i^*$ represents the flux of non-equilibrium internal energy of species *i*. An approximate expression for the energy flux as a product of the gradients in the energy and the viscosity can be obtained from the kinetic theory of gases (e.g. Hirschfelder, Curtiss & Bird 1954). The gradient in energy can itself be expressed in terms of the specific heat at constant volume and the temperature, leading to a heat conductivity coefficient that is the product of viscosity and specific heat. The total heat flux can then be expressed in the form

$$\boldsymbol{q}_i = -\kappa_i^{\mathrm{trn}} \nabla T - \kappa_i^{\mathrm{rot}} \nabla T_i^{\mathrm{rot}} - \kappa_i^{\mathrm{vib}} \nabla T_i^{\mathrm{vib}} \tag{3.2}$$

where κ_i^{trn}, κ_i^{rot} and κ_i^{vib} are the heat-conductivity coefficients due to the translational energy, rotational energy and vibrational energy, respectively, of species *i*. Eucken's correction (e.g. Anderson 1989; Park 1990) to the heat conductivity coefficients takes the form

$$\kappa_i^{\mathrm{trn}} = l_i^{\mathrm{trn}} \mu_i C_{v,i}^{\mathrm{trn}}, \quad \kappa_i^{\mathrm{rot}} = l_i^{\mathrm{rot}} \mu_i C_{v,i}^{\mathrm{rot}}, \quad \kappa_i^{\mathrm{vib}} = l_i^{\mathrm{vib}} \mu_i C_{v,i}^{\mathrm{vib}} \tag{3.3a–c}$$

with $l_i^{\mathrm{trn}} = 5/2$, in analogy with mono-atomic gases, and $l_i^{\mathrm{rot}} = l_i^{\mathrm{vib}} = 1$, empirically. The modified Eucken approximation sets $1/l_i^{\mathrm{rot}}$ equal to the Schmidt number, which has a value of about 5/6 for most intermolecular forces, and undergoes a negligible change with temperature. A more accurate expression for the conductivity coefficients has been derived by Mason & Monchick (1962) using an approximate solution to the semi-classical theory of Wang-Chang & Uhlenbeck (1951). This expression incorporates the effects of inelastic collisions through the inclusion of the relaxation time. If one neglects the very weak dependence of the Schmidt number with temperature, the formula of Mason & Monchick has the form

$$l_i^{\mathrm{trn}} = \frac{5}{2}\left\{1 - \frac{26}{47}\left(\frac{C_{v,i}^{\mathrm{rot}}}{R_i Z_i^{\mathrm{rot}}} + \frac{C_{v,i}^{\mathrm{vib}}}{R_i Z_i^{\mathrm{vib}}}\right)\right\}, \tag{3.4a}$$

$$l_i^{\mathrm{rot}} = \frac{6}{5} + \frac{1}{Z_i^{\mathrm{rot}}}, \tag{3.4b}$$

$$l_i^{\mathrm{vib}} = \frac{6}{5} + \frac{1}{Z_i^{\mathrm{vib}}}, \tag{3.4c}$$

where Z_i^{rot} is the rotational collision number, Z_i^{vib} the vibrational collision number, and R_i is the gas constant for species *i*. We apply equation (3.2) to a single species in the gas mixture, and we obtain values for the conductivity of the mixture itself by applying Wilke's rule (Wilke 1950). This rule is derived from the rigorous kinetic theorry of Chapman and Enskog using simplifications for various collision integrals. We also apply Wilke's rule to calculate the mixture viscosity using species viscosities

given by Sutherland's model based on constants obtained by a best-fit to experimental data (Bertolotti 1997).

The inclusion of the relaxation equations and of the heat-flux expressions into the Navier–Stokes equations leads to the governing equations. These equations are herein presented in a form that includes the bulk viscosity, μ_v, even though the rotational energy is treated as an independent variable. We include the bulk viscosity for the convenience of displaying a single set of general governing equations. It is understood that when the rotational energy is treated as an independent variable, the bulk viscosity is set to zero. For some of our calculations we have reduced the number of independent variables by using the bulk viscosity to approximate the effects of rotational relaxation. In this case the governing equations are obtained by letting T denote the translational and rotational temperature, specifying $\mu_v(T)$, and setting T^{rot} equal to T. The continuity equation, momentum equation, energy equation, the equation for enthalpy, the equation of state, the heat-conduction equation, and the relaxation equations, are, in order,

$$\frac{\partial \rho}{\partial t} + \mathrm{div}[\rho \boldsymbol{v}] = 0, \tag{3.5a}$$

$$\rho \frac{\mathrm{D}\boldsymbol{v}}{\mathrm{D}t} = -\nabla p + 2\mathrm{div}\left[\mu \boldsymbol{D} + (\mu_v - \tfrac{2}{3}\mu)\mathrm{tr}[\boldsymbol{D}]\boldsymbol{I}\right], \tag{3.5b}$$

$$\rho \frac{\mathrm{D}h}{\mathrm{D}t} = -\mathrm{div}[\boldsymbol{q}] + \frac{\mathrm{D}p}{\mathrm{D}t} + (\mu_v - \tfrac{2}{3}\mu)(\mathrm{div}[\boldsymbol{v}])^2 + 2\mu \mathrm{tr}[\boldsymbol{D}\boldsymbol{D}], \tag{3.5c}$$

$$h = C_p^{trn} T + \sum_i c_i (e_i^{rot} + e_i^{vib}), \tag{3.5d}$$

$$p = \rho R_{mix} T, \tag{3.5e}$$

$$\boldsymbol{q} = -\kappa^{trn} \nabla T - \sum_i f_i (\kappa_i^{rot} \nabla T_i^{rot} + \kappa_i^{vib} \nabla T_i^{vib}), \tag{3.5f}$$

$$\rho \frac{\mathrm{D}}{\mathrm{D}t} e_i^{rot} + \frac{\rho}{\tau_i^{rot}} \left(e_i^{rot} - \bar{e}_i^{rot}\right) = \mathrm{div}[\kappa_i^{rot} \nabla T_i^{rot}], \tag{3.5g}$$

$$\rho \frac{\mathrm{D}}{\mathrm{D}t} e_i^{vib} + \frac{\rho}{\tau_i^{vib}} \left(e_i^{vib} - \bar{e}_i^{vib}\right) = \mathrm{div}[\kappa_i^{vib} \nabla T_i^{vib}], \tag{3.5h}$$

where

$$2\boldsymbol{D} = \nabla \boldsymbol{v} + (\nabla \boldsymbol{v})^T$$

is the stretching tensor, $\boldsymbol{I}$ is the identity tensor, c_i are the mass fractions of the species, R_{mix} is the gas constant for the mixture, and f_i are the coefficients computed with Wilke's formula applied to thermal conductivity. The viscosity μ and the conductivities κ^{trn} and κ_i^{rot} are functions of the translational temperature T only. The vibrational energies at equilibrium $\bar{e}_i^{rot}$ and $\bar{e}_i^{vib}$ are given by the classical equilibrium expressions from statistical thermodynamics (e.g. Vincenti & Kruger 1965) evaluated at the translational temperature.

The velocity $\boldsymbol{v}$ satisfies the boundary conditions of no-slip at the wall, and a prescribed value in the free stream. The translational, rotational and vibrational temperatures also match a prescribed value in the free stream. At the wall we assume that there is no net heat transfer. This assumption implies that the body has been given sufficient time to come into thermal equilibrium with the flow field, as is the case, for example, for a vehicle at cruising conditions. Furthermore, both

the translational and rotational temperatures are assumed to be in equilibrium with each other near the wall due to the low velocities there. Thus, the translational and rotational temperatures satisfy the Neumann condition

$$\frac{\partial T}{\partial y} = 0, \quad \frac{\partial T^{\mathrm{rot}}}{\partial y} = 0. \tag{3.6}$$

3.1. *The boundary conditions for vibrational temperature*

The flux of vibrational energy at the wall depends on the efficiency of exchange between the vibrational energy of the molecules and the energy contained in the vibrational motions of the atomic lattice of the surface material. At each collision with the wall, a molecule has a probability f_{acc} of an exchange of kT_i^{v} energy quanta with the wall. The net transfer (averaged over many collisions) is proportional to the difference in the average energy levels of the molecules and the wall. This flux is balanced by the conduction of translational heat away from the wall, which yields the desired wall boundary condition for T_i^{v},

$$\kappa_i^{\mathrm{v}} \frac{\partial T_i^{\mathrm{v}}}{\partial y} + f_{\mathrm{acc}} p \left(\frac{2R_i}{\pi T}\right)^{1/2} (T - T_i^{\mathrm{v}}) = 0. \tag{3.7}$$

The factor f_{acc} is proportional to the accommodation coefficient α_{acc} used in the study of heat convection in rarefied gases (Saxena & Joshi 1989). More precisely, our factor f_{acc} equals the accommodation coefficient $\alpha_{\mathrm{acc}}^{\mathrm{vib}}$ for vibrational energy only. Vines (see Saxena & Joshi 1989) proposed a subdivision of the total α_{acc} into translational, rotational and vibrational portions based on the relative contribution of each energy mode to the total thermal energy,

$$(C_v^{\mathrm{tot}} + R_i/2)\alpha_{\mathrm{acc}} = \alpha_{\mathrm{acc}}^{\mathrm{trn}}(C_v^{\mathrm{trn}} + R_i/2) + \alpha_{\mathrm{acc}}^{\mathrm{rot}} C_v^{\mathrm{rot}} + \alpha_{\mathrm{acc}}^{\mathrm{vib}} C_v^{\mathrm{vib}}. \tag{3.8}$$

With this partition, $\alpha_{\mathrm{acc}}^{\mathrm{vib}}$ contributes from 0% to about 20% to the overall value of α_{acc} for a diatomic molecule, depending on temperature. Furthermore, the total value of α_{acc} for nitrogen is typically between 0.3 and 1, as can be seen in the large collection of experimentally measured values of α_{acc} for different gases and surfaces reported in Saxena & Joshi (1989). Thus, Vines' suggestion yields a value of $\alpha_{\mathrm{acc}}^{\mathrm{vib}}$ between 0.06 and 0.2.

Many of the experimentally measured accommodation coefficients reported in the literature have been computed from the overall heat flux and, thus, the measurements do not distinguish between the amount of energy in the translational and the internal degrees of freedom in the gas molecules leaving the surface. An investigation (Asscher *et al.* 1983), however, employing laser light to probe the vibrational energy of nitric oxide molecules scattered from a platinum crystal surface (111)†, has shown accommodation coefficients for vibrational energy that vary between 0.9 and 0.75 in the surface temperature range of 400 to 1200 K. These results have been obtained in carefully controlled experimental conditions in order to reduce the influence of unwanted phenomena (Somorjai 1994) including contamination of the surface through the adsorption of ambient gas molecules, terraces at the atomic level, surface absorption of gas molecules, and catalysed molecular dissociation. We must be careful, therefore, in giving an over-broad generality to these results, especially when extending the results to the ultra rough and imperfect (at the atomic level), weather-beaten, contaminated, oxidized, or even painted, metallic surfaces used in 'real life' engineering applications exposed to gases at pressures many orders of magnitude greater than those of the

† These indices indicate the orientation of the surface-plane with respect to the crystal lattice.

ultra-high vacuum conditions used in the experiment. One can only make an educated guess for the value of f_{acc} in equation (3.7). For simplicity, we follow Vire's suggestion and set f_{acc} equal to $C_v^{\mathrm{vib}}/C_v^{\mathrm{tot}}$, which produces a value that lies in the reasonable range of 0 to 0.2. We have increased the value to 1 in some computations to measure the sensitivity of the overall boundary-layer stability problem to this parameter and, fortunately, we have found the sensitivity to be weak.

3.2. *The linearized governing equations*

The linear equations governing the evolution of small-amplitude perturbations are constructed following the standard approach for linear stability analysis. Due to the many terms that make up these equations, these lengthy equations will not be reported here. A full listing is given in Bertolotti (1997). The streamwise derivatives of the mean laminar flow are neglected and the small-amplitude perturbations are expressed in normal-mode form to arrive at essentially Orr–Sommerfeld type equations that incorporate the relaxation equations. The spanwise wavenumber β and the frequency ω of the normal-mode ansatz remain constant as the wave is convected downstream, while the complex streamwise wavenumber $\gamma + \mathrm{i}\alpha$ incorporates the growth rate γ and streamwise wavenumber α.

We neglect the weak spatial growth of the mean flow and use governing equations of Orr–Sommerfeld type mainly to facilitate comparisons with the numerous results published in the literature. The effect of the streamwise derivatives of the mean flow on the stability of the disturbances can be studied, for example, with the parabolized stability equations (Bertolotti, Herbert & Spalart 1992; Herbert 1997) but these effects are not central to our main interest.

The stability equations are solved numerically employing a spectral-multi-domain discretization in the wall-normal coordinate. In order to eliminate the possibility of our computations suffering from under-resolution, we have employed a total of 200 Chebyschev polynomials per variable, distributed over 10 domains covering the region extending from the wall to about 15 (or more) boundary-layer heights. In routine calculations assuming thermal equilibrium, half this number of Chebyschev polynomials already provides a fully converged solution.

A successful code validation was performed by comparing the growth rates obtained by multiplying the relaxation rates by 10^{-8} to the growth rates computed with an independent code that used thermal equilibrium (i.e. five independent variables). As a further test, we used our code to calculate the attenuation of planar sound waves in quiescent air. With only the rotational energies active, the code reproduced accurately the experimentally measured attenuation of a planar wave in pure nitrogen at 300 K and one atmosphere, as reported in Thompson (1988). A second study that included water vapour in the air mixture and had the vibrational energies active, reproduced accurately the measured sound-wave attenuation in air with 37% relative humidity also reported in Thompson (1988). These comparisons are presented in Bertolotti (1997).

4. Influence of rotational relaxation on boundary-layer stability

Herein we look at the effect of rotational relaxation on the growth rates of instabilities in the compressible boundary layer over a thin flat plate aligned with the flow. The plate is taken to be infinitely thin to avoid any strong leading-edge shocks, and while in practice the growth of the boundary layer near the leading edge will cause a weak oblique shock, we will avoid considering this phenomenon by taking

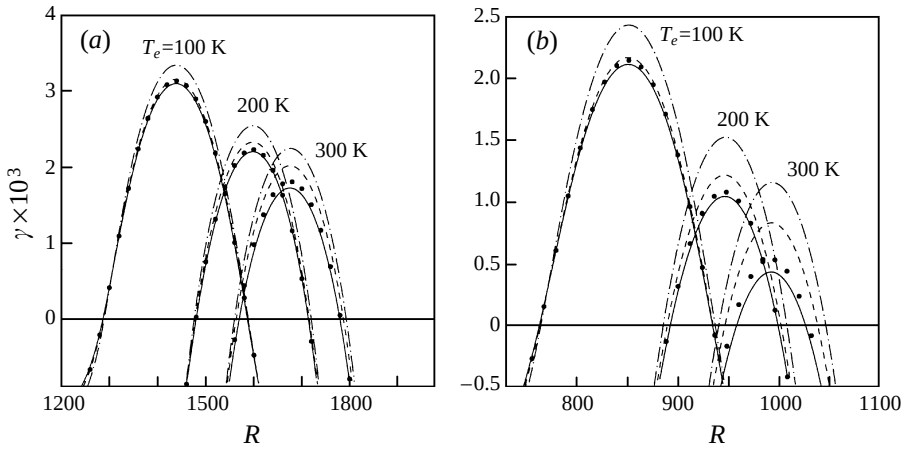

FIGURE 4. Growth rates versus local Reynolds number for a second mode with frequency $F = 150$ (*a*), and $F = 250$ (*b*), at different free-stream temperatures. Solid line, non-equilibrium solution; dashed-dotted line, equilibrium with $\mu_v = 0$; dashed line, equilibrium with $\mu_v/\mu = 0.6$; symbols, equilibrium with μ_v given by (2.4).

our free-stream quantities to be those found outside the boundary layer in the region downstream of the leading edge. The free-stream density is chosen to be 0.31 kg m^{-3}, which corresponds to the density of the US standard atmosphere at 12 000 m of altitude.

In the absence of wave-like oscillations in the flow, the most important parameter for gauging the effect of relaxation is the 'relaxation distance' U_∞/τ, which indicates the spatial extent of the relaxation process at a given speed. At Mach 4.5 and free-stream temperature of $T_\infty = 200$ K, the longest rotational relaxation distance occurs in the free stream and has a value of about 5 μm, which is a few percent of the boundary-layer height, and which is much shorter than the size of the flying object. Thus, we can assume that the laminar base flow has the translational and rotational energies in equilibrium.

Figure 4 displays the growth rates at different free-stream temperatures for a second-mode instability with $\beta = 0$ and non-dimensional frequency $F = 150$ or $F = 250$. The non-dimensional frequency F is defined as

$$F = 10^6\omega^*\mu_\infty/(U_\infty^2\rho_\infty), \tag{4.1}$$

where $\omega^*/(2\pi)$ is in Hz. We adopt this conventional definition of non-dimensional frequency, rather than one based on relaxation time, because the relaxation process is of secondary magnitude in the overall kinematical processes that generate the instabilities.

The growth rates are non-dimensionalized with the viscous length

$$\delta(x) = [\mu_\infty x/(\rho_\infty U_\infty)]^{1/2} \tag{4.2}$$

and are plotted as function of the local Reynolds number

$$R = (\rho_\infty U_\infty x/\mu_\infty)^{1/2} \tag{4.3}$$

based on $\delta(x)$ and free-stream velocity. This Reynolds number depends on the square root of the local Cartesian or surface-oriented x-coordinate.

The damping effect of rotational relaxation can be clearly seen by comparing the

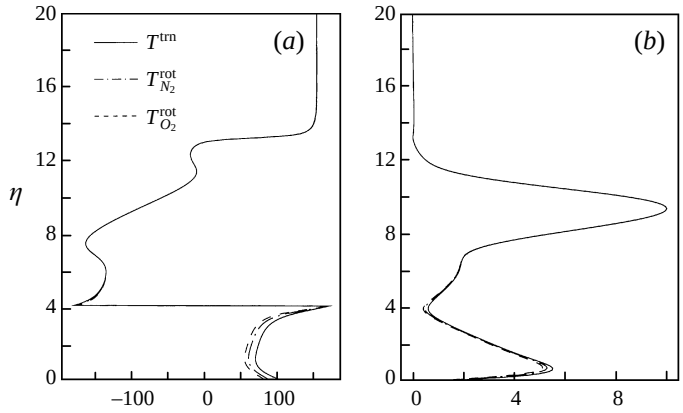

FIGURE 5. Phase (*a*) and modulus (*b*) of the translational and rotational temperatures for a second mode with $\beta = 0$ and $F = 250$, at $R = 980$, Mach $= 4.5$, $T_e = 300$ K. Thin flat plate geometry.

maximum attained by the non-equilibrium solution, denoted by the solid line, and the maximum obtained by the solution computed using the assumption of thermal equilibrium, denoted by the dashed-dotted line. The damping increases with temperature because the rotational relaxation time increases with temperature, causing the product $\omega\tau^{rot}$ to approach one. At $\omega\tau^{rot} = 1$ the dampening effect of rotational relaxation is maximal. The dashed line shows the results obtained with a thermal equilibrium formulation using the usual value for bulk viscosity given by the temperature-independent ratio $\mu_v/\mu = 0.6$. This value is correct at room temperature, but is not at higher temperatures, as discussed earlier. These stability results agree with the non-equilibrium results at the coldest conditions, i.e those corresponding to a free-stream temperature of $T = 100$ K, but disagree at higher temperatures. Using, instead, a bulk viscosity defined by equation (2.4), the stability results closely approach the accurate results given by the non-equilibrium formulation.

In figure 5 we display the phase and amplitude distribution of translational and rotational temperatures for a second mode at frequency $F = 250$ at a location within the amplified region. The phases of the vibrational temperatures of nitrogen and oxygen are clearly different from the translational temperature at distances from the wall below $\eta = 4$, where η is the classic Blasius variable. The distributions, on the other hand, remain quite similar to each other. The phase difference is largest near the wall due to the increase of rotational relaxation time that accompanies the higher temperatures in this region. The fluid temperature is about 300 K in the free stream and 900 K at the wall. The rotational relaxation times vary from 3.4×10^{-9} (5.3×10^{-9}) in the free stream to 2.7×10^{-8} (4.2×10^{-8}) at the wall for nitrogen (oxygen). The corresponding product of disturbance frequency and relaxation time, $\omega\tau$, varies from 0.05 (0.077) in the free stream to 0.40 (0.622) at the wall for nitrogen (oxygen). Clearly, this ratio is order one near the wall.

5. Influence of vibrational relaxation

While rotational relaxation directly influences the growth rate of boundary-layer disturbances by causing the rotational energy to lag behind the translational energy, vibrational relaxation influences the boundary layer stability in an indirect way, namely by changing the mean-flow properties in the boundary layer. The influence

is strongest when the flow field contains a region at, or near, stagnation conditions, followed by a rapid expansion, such as inside wind tunnels and around bodies with a blunt leading edge, whereby the rapid expansion causes the internal energy to freeze in a distribution out of equilibrium. We first compare the mean flow over a thin flat plate in a wind-tunnel flow to that found in free flight and to that computed assuming thermal equilibrium, followed by a comparison of the corresponding stability results. We then turn to the mean flow over a blunt body in atmospheric flow, and to its stability. In all these studies we employ the bulk-viscosity approximation discussed in the previous section to remove the rotational temperatures as independent variables.

5.1. *The mean flow over a thin flat plate*

The supersonic flow in wind tunnels differs in one important way from that found in free flight, namely the flow is initiated from a high-pressure, low-velocity, and high-temperature reservoir. These conditions generate thermal equilibrium in the chamber leading to the nozzle, but once the flow enters the rapid expansion in the nozzle itself, the drop in translational temperature and density, in conjunction with the slow vibrational relaxation rates at low temperatures, freezes the vibrational energy at essentially the value found in the reservoir. The resulting flow has the same total internal energy and stagnation temperature† as the flow in free flight that one wishes to simulate, but has a widely different partition of the total internal energy – the wind-tunnel flow (in the free stream) is colder in the translational temperature, and much hotter in the vibrational temperature. This non-equilibrium flow produces a laminar boundary layer at the model's surface that has different stability characteristics to either the boundary layer found in free flight or computed using the assumption of thermal equilibrium.

To simulate the wind-tunnel flows we set the vibrational temperature of nitrogen and oxygen in the free stream equal to the stagnation temperature. The translational temperature is then computed by subtracting the vibrational energy from the total internal energy. On the other hand, to simulate the free-flight conditions we set the vibrational temperatures in the free stream equal to the translational temperature. The total internal energy (i.e. the stagnation temperature) has the same value in the wind-tunnel and the free-stream cases, hence these two flows are indistinguishable from one another under the assumption of thermal equilibrium. That is, both these flows have equal stagnation temperature, free-stream density, and free-stream velocity, and can be differentiated from one another in the free stream only by the distribution of energy in the internal degrees of freedom.

For reference quantities, we chose the free-stream density $\rho = 0.31$ kg m^{-3}, and equilibrium temperature $T_\infty = 216$ K that correspond to the values found in the US standard atmosphere at an altitude of 14 000 m. The Mach number, based on equilibrium conditions, is chosen as $M = 4.5$, yielding a free-stream velocity of $U_\infty = 1327$ m s^{-1}. The specific heat C_p at equilibrium equals 1007 J kg^{-1} K. Since we use equilibrium quantities for non-dimentionalization, the free-stream values at non-equilibrium conditions do not asymptote to one.

For the equilibrium calculations we employ the well-known similarity solution for the boundary-layer flow (e.g. White 1974). For the non-equilibrium calculations we solve the boundary-layer equations derived from equations (3.5*a*)–(3.5*h*) using Prandtl's formulation. These equations, which form the first-order problem in a

† A wall-temperature probe is also insensitive to the non-equilibrium conditions because the efficient exchange of vibrational energy between the gas and the surface drives the near-wall flow towards equilibrium.

Quantity	Wind tunnel	Free flight	Equilibrium
Stagnation temperature (K)	1041.2	1041.2	1041.2
T wall	4.04	4.33	4.20
T_y wall	0.0	0.0	0.0
T edge	0.772	1.0	1.0
$T_{N_2}^{\mathrm{vib}}$ edge	4.82	1.0	1.0
$T_{O_2}^{\mathrm{vib}}$ edge	4.82	1.0	1.0
Density edge	1.30	1.0	1.0
Viscosity edge	0.798	1.0	1.0
Mach number edge	5.1	4.5	4.5
$\tau_{N_2}^{\mathrm{vib}}$ edge (s)	0.35355	0.1383	0
$\tau_{O_2}^{\mathrm{vib}}$ edge (s)	0.40104	0.1331	0
$\tau_{N_2}^{\mathrm{vib}}$ wall (s)	1.65×10^{-3}	1.22×10^{-3}	0
$\tau_{O_2}^{\mathrm{vib}}$ wall (s)	7.74×10^{-4}	5.89×10^{-4}	0

TABLE 2. Flow properties at $R = 1000$ for a thin, flat plate. The Mach number and other properties computed from stagnation values are equal in the three flows.

matched-asymptotic expansion procedure, are of parabolic character in x and their solution cannot be started from the infinitely sharp leading edge since the equations are singular there. Consequently, the equations are numerically integrated downstream starting at a selected initial location, which we take to be $R = 200$. This particuar location lies sufficiently upstream of the instability region. The initial conditions at $R = 200$ are computed using the self-similar equations for density, velocity, translational temperature, and vibrational temperatures. Using self-similar equations to compute the initial conditions is equivalent to neglecting the small amount of relaxation that takes place in the region between the leading edge and the initial location. The extent of this region is small compared to the extent of the region of instability, and computations made by starting at $R = 200$ and $R = 300$ show that by $R = 600$ the differences in the translational and vibrational temperature profiles are negligible (Bertolotti 1997).

To help compare the characteristics of the wind-tunnel flow with those of the free-flight case and those obtained with the assumption of equilibrium, we present in table 2 the free-stream and wall values of selected quantities.

Figure 6 displays the translational temperature profiles and the N_2 and O_2 vibrational temperature profiles at various streamwise locations, for both the free-flight case and the wind-tunnel case. The Cartesian wall-normal coordinate y is normalized with the (constant) Blasius length δ computed at the location $R = 300$ in order to display the thickening of the boundary layer with streamwise distance.

The main difference between the wind-tunnel case and the free-flight case lies in the free-stream values of the translational and vibrational temperatures. In the free-flight case these temperatures are in equilibrium, but in the wind-tunnel case the vibrational temperatures are frozen at the stagnation temperature, causing the translational temperature to asymptote to 0.772, rather than one, to counter-balance the large amount of energy stored in the vibrational modes. At the wall, the flow is out of equilibrium at the most upstream location shown but rapidly approaches equilibrium as the streamwise coordinate is increased. In particular, by $R = 664$ the translational and vibrational temperatures at the wall reach thermal equilibrium, and remain in equilibrium thereafter. Doubling the value of the accommodation coefficient f_{acc} in equation (3.7) has only a small influence on this development, showing that

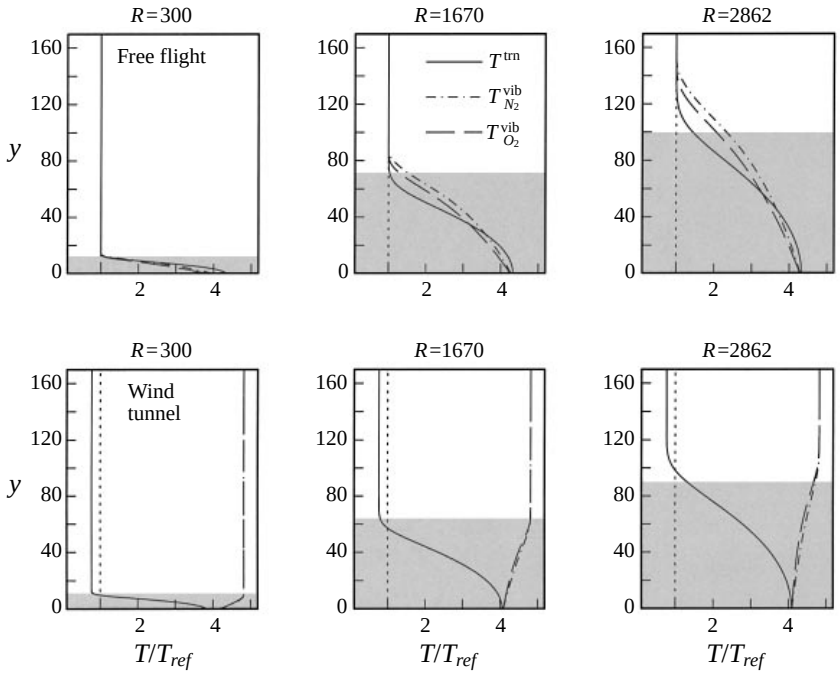

FIGURE 6. Translational temperature T, and vibrational temperature of N_2 and O_2 over a flat plate in free-flight and in wind-tunnel conditions ($M = 4.5$, $T_{ref} = 216$ K). The wall-normal Cartesian coordinate y equals η at $R = 300$). The grey region displays the boundary-layer height based on 99% u-velocity.

the relaxation process at the wall is not sensitively dependent on the value of f_{acc}. In the region between the wall and the free stream, the vibrational temperature profile is affected by two phenomena. First, the profile is drawn towards the translational temperature profile under the action of relaxation, as can be seen in the plots of the wind-tunnel case. Second, the profile is affected by the action of diffusion, as can be seen in the plots for the free-flight case. The effect of diffusion is accentuated by the weakening of the relaxation process away from the wall caused by the rapid decrease of translational temperature. In particular, a large relaxation time τ^{vib} changes equation (3.5*h*) to a diffusion dominated equation having a diffusion rate different from that of translational temperature. The vibrational energy diffuses outwards as long as a gradient exists in the vibrational energy itself and, consequently, the diffusion process continues even outside the (classical) boundary layer. This phenomenon can be seen in the plots for $R = 1670$ and $R = 2862$ in figure 6.

5.2. *The stability results for the flat plate*

The neutral stability diagram in figure 7 shows the domain in the frequency–Reynolds number plane in which the flow is unstable, for both the case of wind-tunnel flows and the case of thermal equilibrium. The areas shaded in grey, which denote stability, and those in white, which denote instability are separated by the neutral curve, and refer to the wind-tunnel conditions. The dashed curve, on the other hand, encloses the unstable region computed under the assumption of thermal equilibrium. The non-dimensional frequency F is defined in equation (4.1), and the local Reynolds number R is defined in equation (4.3). The unstable region at lower frequencies corresponds to Mack's first unstable mode having a wave angle β/α of 60° at $R = 300$. This wave

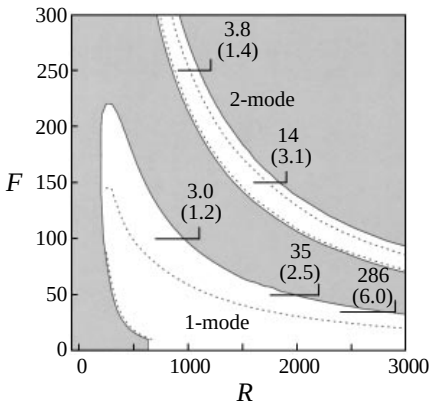

FIGURE 7. Neutral stability diagrams for a thin flat plate in a free stream at Mach 4.5 and temperature of 216 K ($T_{stag} = 1041$ K). The wave angle for the first mode is 60° at $R = 300$. The wave angle for the second mode is 0. The shaded area denotes stability, and the white area denotes instability for the case of wind-tunnel conditions. The neutral curve computed with thermodynamic equilibrium is shown as a dashed line. The numbers show the total amplification of the instability within the unstable region at the frequency marked by the horizontal line. The numbers in parenthesis correspond to the equilibrium calculation. Frequencies below $F = 10$ have not been computed.

angle is close to that of the most amplified disturbances, and, at each frequency, the corresponding dimensional spanwise wavenumber β is held constant at downstream positions (i.e. higher R), in agreement with the wave's behaviour in free flight and in wind tunnels. The upper unstable region corresponds to Mack's second mode of instability. For these modes, the spanwise wavenumber is zero.

The numbers shown at the downstream end of the instability domain in figure 7 denote the total amplification that a wave undergoes in the unstable region at the frequency indicated by the horizontal line. The numbers in parenthesis show the corresponding value obtained assuming thermal equilibrium. Both the first and the second mode are significantly more amplified at the wind-tunnel conditions. In particular, the non-equilibrium increases the total amplification of the second modes up to a factor 4.5 higher than that given by thermal equilibrium. For low-frequency first modes the increase in amplification is significantly larger, yielding an increase of about 47 times at $F = 35$. This is the lowest frequency for which the mode's unstable region lies entirely within our computational domain, and we anticipate that even greater differences in total amplification occur at lower frequencies. The log of the amplification factor of 286 at $F = 35$ is 5.6, and even though this logarithmic value is lower than the value of 9 normally used as the (empirical) value at which transition occurs, the increase in amplification in wind-tunnel flows will undoubtedly affect the location at which nonlinear interaction between modes occurs and, hence, the location of laminar–turbulent transition itself.

The above results were obtained with a free-stream temperature representative of atmospheric flight, but wind-tunnel experiments are often performed at colder free-stream temperatures in order to achieve higher unit Reynolds numbers. These colder flows have a stagnation temperature that is lower than the 1041 K used in the above analysis, hence we cannot conclude that the strong influence of vibrational energy non-equilibrium presented above is found in all wind-tunnel measurements. To highlight this point, we repeat our calculations using the same density of 0.31 kg m^{-3} and free-stream Mach number of $M = 4.5$, but with a free-stream temperature of 100 K

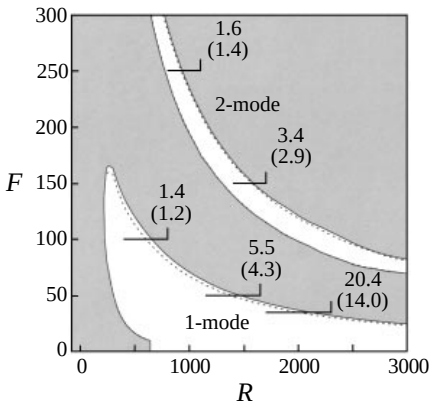

FIGURE 8. As figure 7 but for a temperature of 100 K ($T_{stag} = 500$ K).

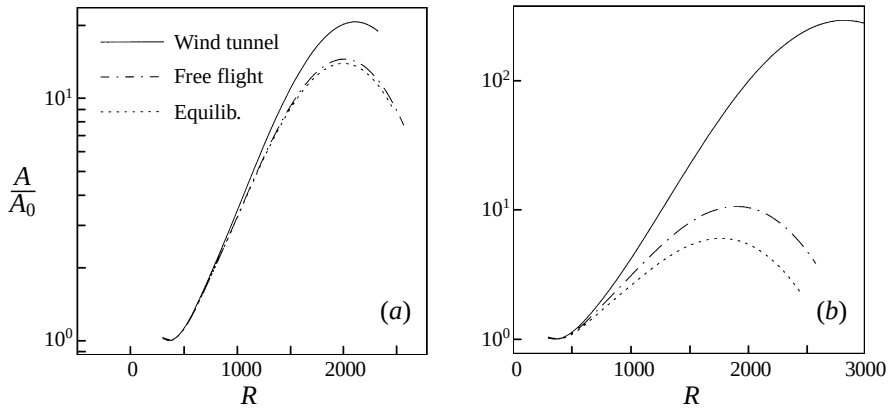

FIGURE 9. Amplitude versus local Reynolds number for a first mode with frequency $F = 35$ for the case of a thin flat plate in a flow at Mach 4.5 and free-stream temperature of 100 K (*a*) and 216 Kelvin (*b*). The corresponding stagnation temperatures are 502 K and 1041 K. The wave angle is 60° at $R = 300$.

in order to obtain a stagnation temperature of 502 K. The resulting neutral stability plot is shown in figure 8. The stagnation temperature found in the reservoir upstream of the wind-tunnel nozzle is not high enough to excite any significant amount of vibrational energy, and, as expected, the difference between the non-equilibrium and equilibrium neutral curves for the flat plate is much smaller than that at the higher temperatures. The additional amplification at the wind-tunnel conditions is only 1.17 times greater than the value obtained using thermal equilibrium for the second mode and 1.5 times for a first mode at $F = 35$. We feel that such differences might be of interest from the academic point of view, but are small in comparison to the influence of other phenomena not addressed in this work, such as the quality of the flow and of the surface finish (i.e. receptivity). We observe, however, that the ultimate objective of wind-tunnel measurements is not to duplicate results calculated using the assumption of thermal equilibrium, but to duplicate the events that take place at free-flight conditions, wherein the high stagnation temperatures are unavoidable.

Figures 9 and 10 compare the mode's amplitude evolution with downstream distance for flows having 100 and 216 K free-stream temperature. In addition to the wind-tunnel and the equilibrium results, we also display the amplitudes obtained for the

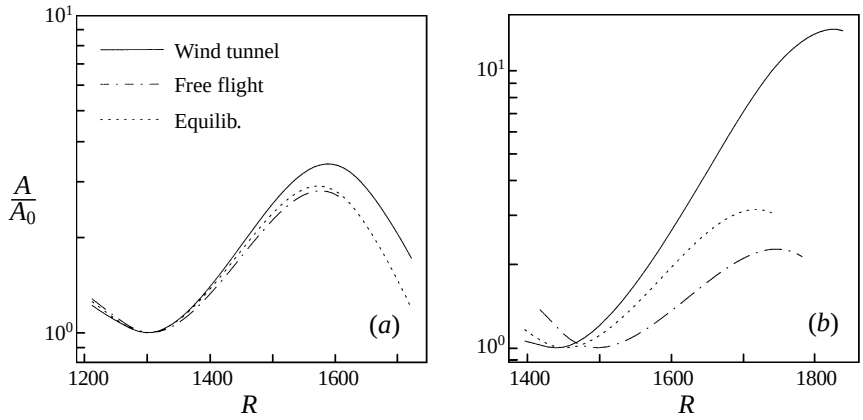

FIGURE 10. Amplitude versus local Reynolds number for a second mode with frequency $F = 150$ for the case of a thin flat plate in a flow at Mach 4.5 and free-stream temperature of 100 K (*a*) and 216 K (*b*). The corresponding stagnation temperatures are 502 K and 1041 K. The wave angle is 0.

free-flight conditions. We emphasize that an equilibrium flow outside the boundary layer in free flight exists only because our plate is assumed to be very thin. In the presence of leading-edge bluntness, the flow will be in non-equilibrium, as discussed in the next section. The results for the atmospheric temperature of 100 K are included only for completeness, since such a low temperature does not exist at any altitude.

The maximum amplification of the first-mode disturbances at $F = 35$ in wind-tunnel conditions with a free-stream temperature of 216 K is much higher than the corresponding amplification either in free flight or under the assumption of thermal equilibrium. The increase in amplification dwarfs the increase in amplification due to the 'non-parallel' effect (i.e. the growth of the boundary layer) that has been the subject of numerous recent studies (for example Bertolotti & Herbert 1991; Chang *et al.* 1991; Wendt, Simen & Hanifi 1995). At $F = 35$ the maximum amplification in wind-tunnel conditions is 4.8 times higher than that computed with equilibrium. At $F = 50$ this difference is 13.8 and for a second mode at $F = 150$ it is back to 4.5, indicating that the influence of vibrational non-equilibrium is strong at all frequencies.

For the first-mode disturbances at $F = 35$ the free-flight conditions produce a higher total amplification than that of equilibrium. For the second mode at $F = 150$ the effect is opposite. The lower amplification obtained for the infinitely thin flat plate in 'free-flight' conditions as compared to equilibrium conditions is consistent with the results reported by Hudson *et al.* (1997). These authors concluded that the effect of thermal non-equilibrium is stabilizing, but now we see that this conclusion is valid only for second-mode disturbances in the idealized case of an infinitely thin, shock-free flat plate. The effect of non-equilibrium on first-mode disturbances is destabilizing, and, more importantly, thermal non-equilibrium in either wind-tunnel conditions or blunt-body flows in free flight is strongly destabilizing for all modes.

Figure 11 displays the streamwise velocity and the translational and vibrational temperature profiles for the first-mode disturbance with $F = 35$ at a location within the unstable region. The vibrational temperatures of the disturbance are smaller than the translational ones, as one would expect from the slow relaxation times for vibrational energy, but their amplitude is much larger than one would estimate based on the relaxation times only. Part of the reason for the large amplitude value is the effect of transport of vibrational energy through convection and diffusion,

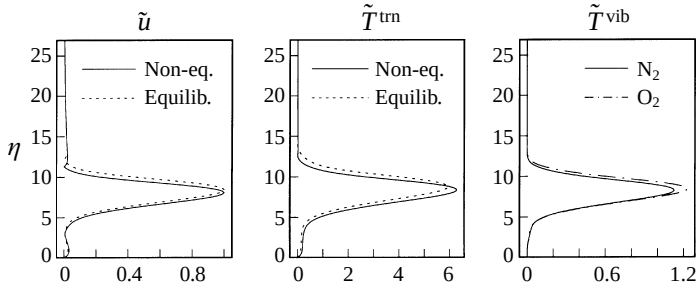

FIGURE 11. Velocity and temperature profiles at $R = 1370$ of a first mode wave with $F = 35$ and wave angle 60° for the case of a thin flat plate in a flow at Mach = 4.5 and $T_e = 216$ K ($T_{stag} = 1041$ K). The dashed line in the $\tilde{u}$ and $\tilde{T}^{trn}$ plots shows the result obtained using thermal equilibrium.

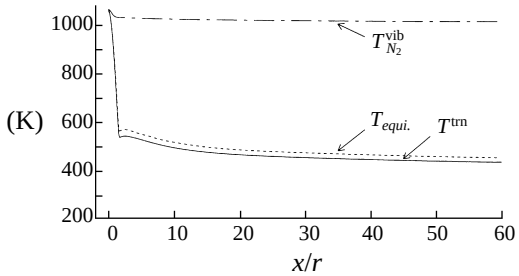

FIGURE 12. Temperatures at the edge of the boundary layer as function of arc-length along the surface of the blunt plate.

combined with a strong variation of the mean-flow vibrational temperature across the boundary layer. From the observation of the temperature profiles, we propose that the destabilizing effect of thermal non-equilibrium in wind-tunnel flows is a combination of both the colder translational temperature in the free stream, and of non-equilibrium effects in the stability process itself.

5.3. *Influence of vibrational relaxation in free flight*

In this section we consider the case of a blunt, adiabatic, flat plate, with a 15 mm nose radius, flying at Mach 4.5 at an altitude of 12 000 m. The inviscid, non-equilibrium flow about the plate has been computed using a shock-capturing Euler code, known as the τ-code, into which the thermal and chemical non-equilibrium processes have been incorporated, Hannemann (1997). The plate length is 60 nose radii in order to include the unstable boundary-layer region.

At the stagnation point the flow is either at, or close to, thermal equilibrium, but as the flow accelerates past the leading edge the density and the translational temperature rapidly drop, causing the vibrational energy of nitrogen and oxygen to freeze. The rapid expansion behaves, effectively, like the nozzle in the wind-tunnel flow. Thereafter, the relaxation rate of the vibrational temperature towards the translational temperature occurs on a length scale that is much greater than the computed domain.

The frozen vibrational energy causes the translational temperature to drop below the value computed with thermal equilibrium, making the boundary layer more unstable. The freezing effect can be seen in figure 12 which shows the surface values of translational and vibrational temperature computed with the Euler code.

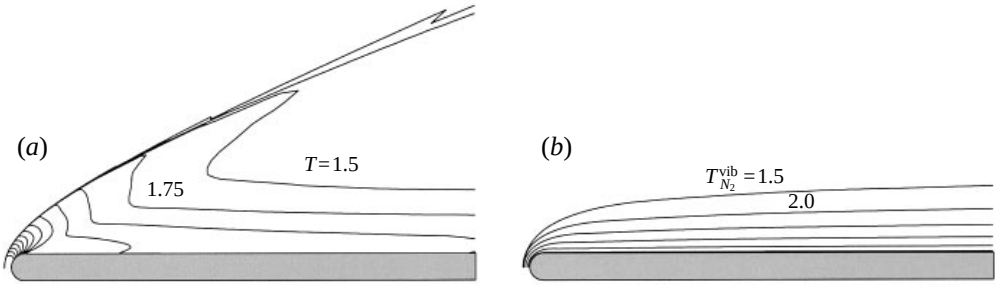

FIGURE 13. Iso-lines of translational temperature and vibrational temperature computed with the non-equilibrium Euler code.

	Blunt plate (free flight)	Thin plate (wind tunnel)	Thin plate (free flight)
Trans. temperature (K)	432	166	216
Vib. temperature N_2 (K)	946	1041	216
(Equil. temperature) (K)	454	216	216
Density kg m^{-3}	0.18	0.31	0.31
Velocity m s^{-1}	1156	1327	1327
Mach number (actual)	2.8	5.1	4.5
(Mach number equilibrium)	2.7	4.5	4.5

TABLE 3. Properties in the flow outside the boundary layer for the blunt plate at $x/r = 50$, and the sharp, thin plate. The Mach number at equilibrium is the value obtained if the flow were allowed to come into thermodynamic equilibrium.

In this and later figures the coordinate x is the surface arc-length measured from the stagnation point, and x/r is the distance normalized with the leading edge radius. The corresponding iso-contour lines of translational temperature and vibrational temperature are shown in figure 13.

Before we discuss the destabilizing effect of the non-equilibrium process, we note that bluntness also has a stabilizing effect on the flow, and this stabilizing effect can dominate over the non-equilibrium effect in certain geometries. The stabilizing effect is mainly due to two reasons. First, the properties at the edge of the boundary layer on the blunt plate are quite different from the corresponding values on the thin plate. Table 3 compares the edge values. The blunt leading edge almost doubles the free-stream translational temperature, halves the Mach number, and halves the density, while leaving the free-stream velocity about equal to the thin-plate case. The values in this table were taken at $x/r = 50$, which lies near the end of our computational domain, hence the effect of bluntness persists far enough downstream to affect the unstable boundary-layer region.

Secondly, the translational temperature, velocity and density at the edge of the boundary layer increase slowly with arc-length. The flow over the flat part of the plate is, thus, slightly accelerated. As a measure of the acceleration, we compute the local Hartree parameter $\beta_H(Q) = (x/Q)(\mathrm{d}Q/\mathrm{d}x)$ based on the streamwise velocity ($Q = U$), the translational temperature ($Q = T^{\mathrm{trn}}$), and the vibrational temperature of nitrogen ($Q = T^{\mathrm{vib}}_{N_2}$). The values are shown in figure 14. The value of $\beta_H(U)$ is about 0.03 over most of the plate's length, and, in the incompressible limit, flows having this value of β_H are known to be more stable than the Blasius flow (for which $\beta_H = 0$).

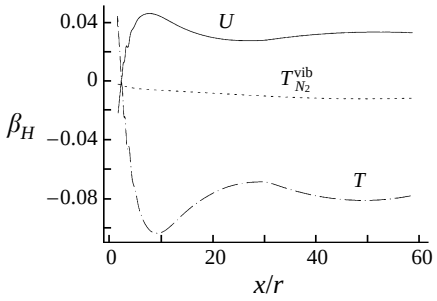

FIGURE 14. Hartree parameters $\beta_H(Q) = (x/Q)\mathrm{d}Q/\mathrm{d}x$ based on streamwise velocity $\beta_H(U)$, translational temperature $\beta_H(T^{\mathrm{trn}})$, and vibrational temperature $\beta_H(T^{\mathrm{vib}}_{N2})$ at the edge of the boundary layer.

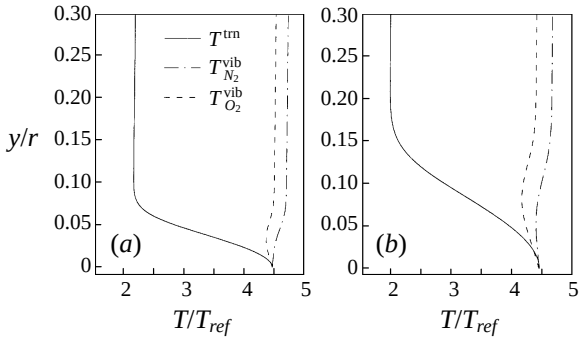

FIGURE 15. Laminar mean-flow profiles of translational and vibrational temperatures as function of wall normal distance y non-dimensionalized with the nose radius ($r = 15$ mm), at streamwise locations (*a*) $x/r = 15$ and (*b*) $x/r = 38$. The reference temperature is 216 K.

Thus, bluntness produces free-stream conditions at the edge of the boundary layer that have a stabilizing effect on the boundary layer itself. Counteracting these stabilizing effects of bluntness are at least two destabilizing effects that increase in strength with increasing nose bluntness, namely the entropy layer instability and thermal non-equilibrium. The first effect is not addressed in the present investigation (see Dietz & Hein (1998)). Like in the flat-plate case previously addressed, the destabilizing influence of vibrational energy relaxation stems from a modification of the laminar mean flow. The computed boundary-layer temperature profiles at two streamwise locations are shown in figure 15. The profiles resemble the profiles over the thin plate in wind-tunnel conditions (see figure 6), in which the translational and vibrational temperatures are in (or near) equilibrium at the wall, and reach widely different values in the free stream.

The streamwise amplitude evolution for three first-mode waves (no second-mode waves were found within the computed domain) with different frequency are shown in figure 16. The spanwise wavelength has been chosen to maximize growth, and gives wave angles (β/α) of about 60°. The dashed lines show the results computed using thermodynamic equilibrium. The destabilizing influence of non-equilibrium produces a total amplification that is just about double that computed with thermal equilibrium.

This increase in total amplification could be relevant in the transition-reversal phenomena. It has been observed in experiments (Ericsson 1988) that increasing

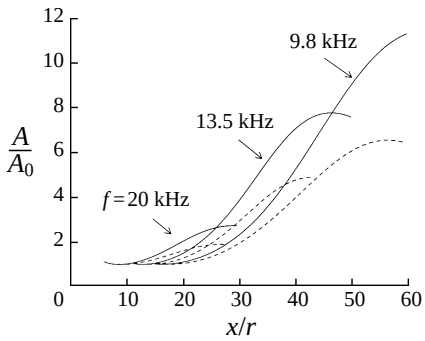

FIGURE 16. Amplification curves versus arc-length along the surface of the blunt flat plate, non-dimensionalized with the nose radius (15 mm), for the three first-mode waves with different frequencies. The solid lines and the dashed lines show the non-equilibrium and the equilibrium results, respectively.

bluntness first stabilizes the flow, pushing the onset of turbulence farther downstream, but after a certain value, increasing the bluntness (i.e. the nose radius) causes the transition onset to move upstream again. This phenomenon is referred to as transition reversal, and lies outside the scope of the present work. Indeed, the effects of increasing bluntness on transition could be due to a combination of phenomena not considered herein, including, for example, the generation of longitudinal streaks in the boundary layer due to turbulence in the outer flow. Entropy modes could also play a role. Our study shows, nevertheless, that the generation of thermodynamic non-equilibrium is one of the destabilizing effects of bluntness.

In view of the practically ubiquitous use of the thermal equilibrium model in current stability investigations, the main conclusion to be drawn from our study of the blunt flat plate is the significant discrepancy between non-equilibrium and equilibrium solutions, as shown in figure 16. Our investigation has used the linearized stability equations, thus has neglected the nonlinear phenomena that are necessary to bring the flow into turbulence. However, based on the existing knowledge on the sensitivity of the transition physics to the amplitude of the disturbances acquired in incompressible flows (e.g. Herbert 1988) we can anticipate that the added amplification caused by thermal non-equilibrium could have a strong influence on the transition location by either anticipating the location of nonlinear mode interactions (here mode is synonymous with 'disturbance'), or, in limiting cases, by causing transition where equilibrium results would predict a laminar flow.

6. Conclusions

The influence of rotational and vibrational energy relaxation on the stability of boundary layers in supersonic flows is investigated using the full thermal non-equilibrium equations.

The two main results are that (*a*) the bulk viscosity approximation used in past investigations is an adequate model for the influence of rotational relaxation when an accurate temperature dependence of the bulk viscosity (derived herein) is used, and (*b*) vibrational relaxation has a large destabilizing influence that has been overlooked by previous investigations, with the de-stabilizing influence being pronounced in boundary layers downstream of a blunt leading edge (both in wind-tunnel flows and in free flight), and in boundary layers over the idealized sharp and thin flat plate in

wind-tunnel flows. Only for the case of the idealized thin plate in free-flight conditions does the influence of vibrational relaxation become weak, and slightly stabilizing for second-mode instabilities, in agreement with the one previous investigation that has considered thermochemical non-equilibrium. For practical geometries, having measurable thickness and a leading edge, the effect of non-equilibrium is strong.

The author would like to thank a number of people who have helped during the course of this work, especially Dr Volker Hannemann at DLR Göttingen for generating and providing the Euler solution of the blunt-plate problem, and for carefully reviewing this manuscript; and including Dr Georg Eitelberg and Dr Walter Beck for supplying technical details on flow measurements in the Göttinger high-enthalpy wind tunnel; Profesor Joseph R. Manson at Clemson University for information about gas–surface interactions and accommodation coefficients; Stefan Hein at DLR Göttingen for information on the transition-reversal phenomenon; and Dr Uwe Dallmann for general support.

REFERENCES

Anderson, J. D. Jr. 1989 *Hypersonic and High Temperature Gas Dynamics*. McGraw-Hill.

Andersen, W. H. & Horning, D. F. 1959 The structure of shock fronts in various gases. *Molecular Phys.* **2**, 49.

Asscher, M., Guthrie, W. L., Lin, T. H. & Somorjai, G. A. 1983 Energy redistribution among internal states on nitric oxide molecules upon scattering from Pt(111) crystal surface. *J. Chem. Phys.* **78**, 6992.

Bass, H. E., Sutherland, L. C., Piercy, J. & Evans, L. 1984 Absorption of sound in the atmosphere. In *Physical Acoustics: Principles and Methods* (ed. R. N. T. W. P. Mason), vol. xvii, pp. 145–232. Academic.

Bauer, H. J. 1965 Phenomenological theory of the relaxation phenomena in gases. In *Physical Acoustics: Principles and Methods* (ed. R. N. T. W. P. Mason), vol. ii.a, pp. 47–131. Academic.

Belikov, A. E. & Sharafutdinov, G. R. 1995 Rotational relaxation time in free jets of He + N_2 mixtures. *Chem. Phys. Lett.* **241**, 209–214.

Bertolotti, F. P. 1997 The influence of rotational and vibrational energy relaxation on the stability of boundary layers in supersonic flows. *Tech. Rep.* DLR-FB-97-18. Deutsches Zentrum für Luft und Raumfahrt, D-37073 Göttingen, Germany.

Bertolotti, F. P. & Herbert, Th. 1991 Analysis of the linear stability of compressible boundary layers using the PSE. *Theor. Comput. Fluid Dyn.* **3**, 117–124.

Bertolotti, F. P., Herbert, Th. & Spalart, P. R. 1992 Linear and nonlinear stability of the Blasius boundary layer. *J. Fluid Mech.* **242**, 441–474.

Brout, R. 1954 Rotational energy transfer in diatomic molecules. *J. Chem. Phys.* **22**, 1189.

Chang, C. L., Malik, M. R., Erlebacher, G. & Hussaini, M. Y. 1991 Compressible stability of growing boundary layers using the parabolized stability equations. *AIAA Paper* 91-1636.

Chang, C. L., Vinh, H. & Malik, M. R. 1997 Hypersonic boundary-layer stability with chemical reactions using PSE. *AIAA Paper* 97-2012.

Clarke, J. F. & McChesney, M. 1964 *The Dynamics of Real Gases*. Butterworths.

Connor, J. V. 1958 Ultrasonic dispersion in oxygen. *J. Acoust. Soc. Am.* **30**, 297–300.

Dietz, G. & Hein, S. 1998 Investigation of entropy-layer instabilities over a blunted flat plate in supersonic flow. *Phys. Fluids* (Letters) submitted for publication.

Ericsson, L. E. 1988 Effect of nose bluntness and cone angle on slender-vehicle transition. *AIAA J.* **26**, 1168–1174.

Evans, L. B., Bass, H. E. & Sutherland, L. C. 1971 Atmospheric absorption of sound: theoretical predictions. *J. Acoust. Soc. Am.* **51**, 1565–1575.

Gaydon, A. G. & Hurle, I. R. 1963 *The Shock Tube in High-Temperature Chemical Physics*. Chapman and Hall.

Germain, P. D. & Hornung, H. G. 1997 Transition on a slender cone in hypervelocity flow. *Exps. Fluids* **22**, 183–190.

Greenspan, M. 1959 Rotational relaxation in nitrogen, oxygen, and air. *J. Acoust. Soc. Am.* **31**, 155.

Hannemann, V. 1997 Numerische Simulation von Stoß-Stoß-Wechselwirkungen unter Berücksichtigung von chemischen und thermischen Nichtgleichgewichtseffekten. *Tech. Rep.* DLR-FB-97-07. Deutsches Zentrum für Luft und Raumfahrt.

Henderson, M. C., Herzfeld, K. F., Bry, J., Coakley, R. & Carriere, G. 1968 Thermal relaxation in nitrogen with wet carbon dioxide as impurity. *J. Acoust. Soc. Am.* **45**, 109–114.

Herbert, Th. 1988 Secondary instability of boundary layers. *Ann. Rev. Fluid Mech.* **20**, 487–526.

Herbert, Th. 1997 Parabolized stability equations. *Ann. Rev. Fluid Mech.* **29**, 245–283.

Herzfeld, K. F. & Litovitz, T. A. 1959 *Absorption and Dispersion of Ultrasonic Waves*. Academic.

Hirschfelder, J. O., Curtiss, C. F. & Bird, R. B. 1954 *Molecular Theory of Gases and Liquids*. John Wiley and Sons.

Hudson, M. L., Chokani, N. & Candler, G. V. 1997 Linear stability of hypersonic flow in thermochemical non-equilibrium. *AIAA J.* **35**, 958–964.

Landau, L. & Teller, E. 1936 Zur Theorie der Schalldispersion. *Phys. Z. Sowjet* **10** (1), 34.

Mack, L. M. 1965 Computation of the stability of a laminar boundary layer. In *Methods in Computational Physics* (ed. M. R. B. Alder & S. Fernbach). Academic.

Mason, E. A. & Monchick, L. 1962 Heat conductivity of polyatomic and polar gases. *J. Chem. Phys.* **36**, 1622–1639.

Monk, R. G. 1969 Thermal relaxation in humid air. *J. Acoust. Soc. Am.* **46**, 580–586.

Nerushev, A. & Novopashin, S. A. 1997 Rotational relaxation and transition to turbulence. *Phys. Lett.* A **232**, 243–245.

O'Neal, C. & Brokaw, R. 1963 Relation between thermal conductivity and viscosity for nonpolar gases. II. Rotational relaxation of polyatomic molecules. *Phys. Fluids* **6**, 1675–1682.

Pack, R. T. 1980 Analytic estimation of almost resonant molecular energy transfer due to multipolar potentials. VV processes involving CO_2. *J. Chem. Phys.* **72**, 6140–6152.

Park, C. 1990 *Non-equilibrium Hypersonic Aerothermodynamics*. John Wiley and Sons.

Parker, J. G. 1959 Rotational and vibrational relaxation in diatomic gases. *Phys. Fluids* **2**, 449–462.

Pierce, A. 1981 *Acoustics: An Introduction to its Physical Principles and Applications*. McGraw-Hill.

Raff, L. M. & Winter, T. G. 1969 Origin of the temperature dependence of the ultrasonic "rotational relaxation" time. *J. Chem. Phys.* **48**, 3992–4000.

Robben, F. & Talbot, L. 1966 Experimental study of the rotational distribution function of nitrogen in a shock-wave. *Phys. Fluids* **9**, 653–661.

Rosser, W. A. & Gerry, E. T. 1969 De-excitation of vibrationally excited $CO_2^*(v_3)$ by collisions with He, O_2 and H_2O. *J. Chem. Phys.* **51**, 2286–2287.

Saxena, S. C. & Joshi, R. K. 1989 Thermal accommodation and absorption coefficients of gases. In *CINDAS Data Series on Material Properties*, Vol. II-1 (ed. C. Y. Ho). Hemisphere.

Shuler, K. E. 1959 Relaxation processes in multi-state systems. *Phys. Fluids* **2**, 442–448.

Somorjai, G. A. 1994 *Introduction to Surface Chemistry and Catalysis*. John Wiley and Sons.

Stuckert, G. K. 1991 Linear Stability of Hypersonic, Chemically Reacting Viscous Flows. PhD thesis, Arizona State University.

Stuckert, G. & Reed, H. L. 1994 Linear disturbances in hypersonic, chemically reacting shock layers. *AIAA J.* **32**, 1384–1394.

Thompson, P. A. 1988 *Compressible-Fluid Dynamics*. Advanced Engineering Series, Irving H. Shames, Consulting Editor, Library of Congress Catalog Number 79-148996.

Vincenti, W. G. & Kruger, C. H. 1965 *Introduction to Physical Gas Dynamics*. Wiley.

Wang-Chang, C. S. & Uhlenbeck, G. E. 1951 Transport phenomena in polyatomic gases. *University of Michigan Engineering Res. Rep.* CM 681.

Wendt, V., Simen, M. & Hanifi, A. 1995 An experimental and theoretical investigation of instabilities in hypersonic flat plate boundary layer flow. *Phys. Fluids* **7**, 877–887.

White, A. H. 1974 *Viscous Fluid Flow*. McGraw-Hill.

Wilke, C. R. 1950 A viscosity equation for gas mixtures. *J. Chem. Phys.* **18**, 517–519.

Yamazaki, S., Masahiro, T. & Yoshiyasu, F. 1981 Rotational relaxation in free jet expansion of N_2 from 300 to 1000 K. *J. Chem. Phys.* **74**, 4476–4479.